Research Square

Preprints are preliminary reports that have not undergone peer review.
They should not be considered conclusive, used to inform clinical practice,
or referenced by the media as validated information.

Resource utilization and recycling of petroleum-contaminated soil by pyrolysis as persulfate activator

Yaping Liao
Changzhou University
Hang Gao
Changzhou University
Mingxin Wang (wmxcau@163.com)
Changzhou University https://orcid.org/0000-0001-8367-7970
Jinjuan Xue
Changzhou University
Meng Yao
Changzhou University

Research Article

Keywords: petroleum-contaminated soil, pyrolysis, remediation, graphitic carbon, persulfate, acute toxicity

Posted Date: June 13th, 2022

DOI: https://doi.org/10.21203/rs.3.rs-1659728/v1

License: This work is licensed under a Creative Commons Attribution 4.0 International License.
Read Full License

Abstract

Oxygen-limited pyrolysis was used to simultaneously remediate and convert petroleum-contaminated soil (PCS) to carbonized soil (CS), which is subsequently reused as a persulfate (PS) activator. The effects of pyrolysis temperature and retention time on the harmlessness of PCS and the PS activation efficiency of CS for aniline (AN) degradation were investigated. When the pyrolysis temperature is 500°C and the retention time is 60 min, the total petroleum hydrocarbon removal rate of PCS and the TOC concentration of CS extracts were 98.96% and 10.2 ppm, respectively. The acute toxicity of CS extracts was classified as non-toxic. The degradation efficiency of AN was up to 96.09% within 6 h. After CS was reused five times, the removal rates of AN and TOC were 53.73% and 51.54%, respectively. The residual organic carbon in CS mainly exists as graphitized carbon, which has good stability and no acute toxicity. The main active species was holes, followed by singlet oxygen. $S_2O_8^{2-}$ is adsorbed on the surface of the positively charged CS and then reduced by electron donor groups to generate holes, which may accelerate electron transfer and facilitate the oxidative degradation of AN. This research provides an innovative alternative disposal strategy for PCS-derivatives treated by pyrolysis, which can simultaneously achieve efficient remediation and high-value reuse of PCS.

1. Introduction

About 10–25 million tons of petroleum products are leaked globally every year, and more than 98% of medium-scale spills occur on land (Gao and Zygourakis 2019; Song et al. 2019). The petroleum hydrocarbon pollutants entering the soil are gradually and closely adsorbed by the organic matter and clay minerals (Vidonish et al. 2016b). With the extension of time, the bioavailability of pollutants shows a downward trend, and the removal difficulty gradually increases (Lyu et al. 2019). The scale of China's petrochemical industry is huge, and leakage accidents in petrochemical enterprises often occur. There is an urgent need for green, rapid, and low-cost treatment and disposal technologies that enable efficient remediation and high-value reuse of PCS.

The treatment technologies currently used in PCS remediation projects can be simply divided into physicochemical remediation technology (McAlexander et al. 2015) and bioremediation technology (Mishra et al. 2021). Physicochemical treatment techniques are highly efficient and require a short treatment time, and are usually used in heavily polluted soils (Kim et al. 2019; Liu et al. 2021). However, physicochemical remediation technologies, such as advanced oxidation (Mustapha et al. 2021), and solvent extraction (Wu et al. 2013), need to consume a lot of chemical agents, and the waste liquid produced by them needs to be treated up to standard. Therefore, the cost of physicochemical technology is generally high. Bioremediation technology is cheaper, but the time required is long, and it is usually applied to lightly polluted soils.

Studies have shown that pyrolysis can efficiently remove petroleum hydrocarbon pollutants in PCS (Vidonish et al. 2016b; Liu et al. 2021). At the same time, the pyrolysis method can recover some fuel oil from the PCS (Li et al. 2018), which can be used to compensate the energy consumption of the pyrolysis

process and reduce the remediation cost. Therefore, pyrolysis is an ideal remediation technique for PCS. The disposal of derivatives from PCS treated by pyrolysis is another important issue to consider. However, currently the derivatives is often used as backfill for construction projects, sent to landfills, or for reclamation and reuse (Liu et al. 2020; Li et al. 2021; Lassalle et al. 2021). In fact, the economic benefits of above-mentioned disposal and reuse value are low, and the valuable components in PCS cannot be fully exploited.

Conventional cleaning soil usually contain components with catalytic properties such as clay minerals, metal oxides, and amorphous carbon. However, clay minerals and metal oxides in soil have high crystallinity and low catalytic activity under natural conditions. Compared with conventional clean soil, PCS contains a large amount of organic matter and organic pollutants (Ren et al. 2020; Liu et al. 2021). Pyrolysis can convert them into amorphous carbon or graphitized carbon with high stability and non-toxicity (Huang et al. 2021; Kohantorabi et al. 2021; Van Luan et al. 2020). Therefore, the PCS-derived material by pyrolysis can be regarded as a mineral/char composite material (CS). Many studies have used clay minerals, metal oxides and amorphous carbon as heterogeneous catalysts for persulfate, and have achieved good catalytic oxidation performance (Wu et al. 2018; Kou et al. 2021). We supposed CS is a highly efficient persulfate activator for degradation of organic pollutants.

Thus, in this study, the PCS was treated by pyrolysis and the obtained derivatives (CS) were used to activate persulfate oxidation for aniline (AN) degradation. The catalytic properties and recycling efficiency of CS on persulfate activation were investigated, the degradation kinetics of AN was analyzed, the main active species in the reaction system were identified, and the mechanism of pyrolysis-induced catalytic activity of CS was revealed. This study aims to provide a high-value reuse and recycling strategy for pyrolytic derivatives from PCS.

2. Materials And Methods

2.1. Experimental materials

PCS was collected from a site contaminated by a chemical plant in Shenzhen, China (5 years after the oil leak, the total petroleum hydrocarbon [TPH] content was 256125 mg/kg), sealed, and stored in a plastic bag. The large particles of gravel and other debris were selected and removed for later use. Aniline (C_6H_7N, ≥ 99.5%) was purchased from Shanghai Runjie Chemical Reagent Co., Ltd. Sodium persulfate ($Na_2S_2O_8$, ≥ 98%), sodium hydroxide (NaOH, ≥ 96%), tetrachloroethylene (C_2Cl_4, IR special chromatographic purity), glucose solution ($C_6H_{12}O_6{\cdot}H_2O$, AR), mercury sulfate ($HgSO_4$, AR), potassium dichromate ($K_2Cr_2O_7$, AR), sulfuric acid (H_2SO_4, AR), sodium thiosulfate, isopropanol (C_3H_8O, AR), tert-butanol ($C_4H_{10}O$, AR), chloroform ($CHCl_3$, AR), furfuryl alcohol ($C_5H_6O_2$, AR), and ethylene diamine tetraacetic acid ($C_{10}H_{16}N_2O_8$, AR) were obtained from Sinopharm Chemical Reagent Co., Ltd. Methanol (HPLC) was acquired from Sigma (USA). Ultrapure water produced by an ultrapure water machine (Milli-Q) was used as experimental water.

2.2. Pyrolytic treatment of PCS

In brief, 10 g of PCS was placed in a quartz ark and then transferred to the tube furnace (OTS-1200X-S 1200A, Hefei Kejing Material Technology Co., Ltd., Hefei, China) with continuously flowing inert gas N_2 (60 mL·min^{-1}) throughout the entire pyrolysis process. Temperature and time were recorded using the tube furnace thermocouple to ensure that the set conditions were reached. Prior to pyrolysis, N_2 (> 100 mL·min^{-1}) was continuously introduced for 5 min to remove the air in the tube furnace and ensure the oxygen-free environment required for pyrolysis. Oxygen-limited pyrolysis temperature (300°C, 400°C, 500°C, 600°C, 700°C, and 800°C) and retention time (15, 30, 45, 60, 90, and 120 min) at a heating rate of 10°C·min^{-1} were established. After the process ended, the system was first cooled down to 25 ± 2°C, and the nitrogen and tube furnace were then turned off. The collected soil was washed with ultrapure water, filtered to remove ash, frozen in the refrigerator for more than 24 h, transferred to a freeze dryer (FD-1A-50, Beijing Boyikang Experimental Instrument Co., Ltd., Beijing, China) for drying for more than 24 h, collected and mixed, and stored in a vacuum glove box. For the pyrolysis tube, a rubber ring was tightly sealed inside to prevent gas from escaping, and a gas outlet was placed at the right end to facilitate gas discharge. According to their differences in pyrolysis temperature and retention time, the obtained samples were named CS_{X-Y} (X = temperature [°C], Y = retention time [min]).

2.3. CS-activated PS oxidation experiment

A series of batch experiments was conducted to evaluate the effect of CS-activated PS, pyrolysis temperature, retention time, and CS and PS dosages on AN degradation. All reactions in the AN degradation experiment were carried out at room temperature (25 ± 2°C), 100 mg·L^{-1} AN concentration, 100 mL solution, and 6 h reaction time unless otherwise specified. CS (dose: 0, 1, 2, 3, 4, and 5 g·L^{-1}) was added to a sealed glass conical flask (150 mL) and mixed first with AN solution to prevent chemical oxidation and then with PS (dose: 0, 1, 2, 3, 4, and 5 g·L^{-1}). The reaction was carried out at a constant temperature shaking box at a speed of 200 rpm·min^{-1}, and all experiments were carried out in duplicate. Liquid samples were collected at different time intervals, and 10 g·L^{-1} sodium thiosulfate was added to terminate the reaction. The samples were filtered through a syringe filter (0.22 μm, Shanghai Anpu Experimental Technology Co., Ltd., Shanghai, China) and stored in a refrigerator at 4°C for subsequent testing.

With the addition of isopropanol (IPA), methanol (MEOH), tert-butanol (TBA), chloroform (CF), furfuryl alcohol (FA), ethylenediaminetetraacetic acid (EDTA) as probe materials, the types of free radicals were identified to determine their impact on organic matter degradation. IPA was used as the quencher for SO_4^{-}· and ·OH, MEOH for SO_4^{-}·, TBA for ·OH, CF for $\cdot O_2^-$, FA for $^1O_2$, and EDTA for holes.

Recycling experiments were conducted to evaluate the potential applications of the recycled CS. After each cycle of PS activation by CS and AN degradation by PS, the reaction solution was centrifuged at 8000 rpm·min^{-1} for 3 min, the liquid was removed, and CS was recovered. Fresh AN solution was added to

perform the shaking experiment again. The above steps were repeated several times to investigate the recycling effect of CS.

2.4. Measurement method and material characterization

AN concentration was determined by high-performance liquid chromatography (HPLC, 1260II, Agilent, USA), and a Waters Atlantis T3 column (2.1mm×50 mm, 3 μm) was used for separation. The mobile phase consisted of 70% methanol (mobile phase A) and 30% ultrapure water (mobile phase B). In brief, 5 μL of the sample was injected and measured for 4 min at a ultraviolet detection wavelength of 280 nm, a column temperature of 25°C, and a flow rate of 0.4 $mL \cdot min^{-1}$.

The change in total organic carbon (TOC) content was used to reflect the mineralization degradation efficiency of AN, and the potassium dichromate oxidation spectrophotometric method (HJ 615–2011) was applied to determine the TOC content in the water samples as follows. First, 30mL of the water sample was placed in the digestion tube of the graphite furnace (Gr20 type, Shanghai Shengsheng Automatic Analytical Instrument Co., Ltd., Shanghai, China), added with 0.1 g of mercury sulfate and 5mL of potassium dichromate solution with a concentration of 0.27 $mol \cdot L^{-1}$ and shaken well. Afterward, 7.5mL of sulfuric acid solution was added, the mixture was shaken gently, heated at 135°C for 30 min, removed from the heat, and cooled to room temperature in a water bath. Ultrapure water was added to each digestion tube to obtain a volume of 50mL and used after cooling to room temperature. The samples were measured at a wavelength of 585 nm in a fully automatic scanning ultraviolet-visible photometer (UV-3000PC, Shanghai Maple Instruments Co., Ltd., Shanghai, China).

TPH concentration was used as an indicator to measure the oil content of PCS and was determined by an infrared spectrophotometer (EP-900, Beijing Bohaixingyuan Instrument Co., Ltd., Beijing, China) as follows. In brief, 0.1 g (± 0.0001 g) of the original and pyrolyzed PCS samples were placed in a 50 mL Erlenmeyer flask and added with 10 mL of C_2Cl_4. The mouth of the bottle was sealed, and the bottle was shaken in a constant temperature shaking box for 30 min and allowed to stand for stratification. Glass fiber microporous membrane (diameter 60mm, pore size 0.45 μm) was used to filter the supernatant in a glass funnel (the soil remained in the Erlenmeyer flask) and collect the filtrate in a 50 mL colorimetric tube. Afterward, 10 mL of C_2Cl_4 was continuously added to the Erlenmeyer flask, and the above experimental steps were repeated. Finally, the glass rod and Erlenmeyer flask were rinsed with a small amount of C_2Cl_4, and their contents were poured into the funnel, filtered into the corresponding colorimetric tubes, and diluted to 25 mL volume.

The TOC content in the CS extracts was measured to determine the leaching risk of CS (Li et al. 2018). In brief, 2.0 g (± 0.0001 g) of soil was placed in a 50 mL Erlenmeyer flask and added with 15 mL of ultrapure water to extract the soluble organic matter (SOM) from the soil. The temperature of the constant temperature shaking box was set to 25°C, and the rotation speed was 200 $rpm \cdot min^{-1}$. After 12 h of shaking, the supernatant was transferred to a plastic centrifuge tube and centrifuged (LG-20W, Beijing Jingli Centrifuge Co., Ltd., Beijing, China) at a rotation speed of 8000 $rpm \cdot min^{-1}$ for 10 min. The prepared

water sample was subjected to potassium dichromate oxidation-spectrophotometry (HJ 615–2011) to determine the TOC of the CS extracts.

A portable water toxicity analyzer (BX-LID-P, Hunan Bixiao Technology) was used to detect the acute toxicity of PCS and CS extracts to determine the impact of pyrolysis conditions on the harmlessness of PCS. The specific method was as follows. The luminescent bacteria (*Vibrio fischeri*) freeze-dried powder was placed in the freezing layer of a refrigerator below − 12°C, removed, and immediately mixed with the bacterial resuscitation solution (refrigerated at 4°C) for recovery. The osmotic pressure of the samples (N, taken from the samples used in the SOM measurement) was then adjusted. Afterward, 0.5 mL of bacterial solution was added to each test tube (N + 1), 0.5 mL of negative control solution was added to the first test tube, and 0.5 mL of osmotic pressure-adjusted sample was added to the rest of the test tubes. After 15 min of mixing, the bioluminescence intensity was measured sequentially. After the test was completed, the relative inhibition rate was calculated to indicate the magnitude of toxicity, and the relative luminous intensity inhibition rate (IR%) was calculated by Eq. (1):

$$\frac{S_0 \times C_f - S_t}{S_0 \times C_f} \times 100\%, \quad (1)$$

where IR% is the relative luminescence intensity inhibition rate, %; St is the sample luminescence intensity, the number of photons; S_0 is the negative control luminescence intensity, the number of photons; and C_f is the correction coefficient.

The contents of C, H, O, N, and S in the soil samples were analyzed using an elemental analyzer (vario EL cube, Elementar, Germany). The valence states of the elements were determined by X-ray photoelectron spectroscopy (XPS) (Axis Ultra DLD, Thermo Fisher Scientific, USA). The high-resolution spectra of O1s and C1s were fitted by XPS Avantage 5.948 software to verify the structural characteristics of the material, and the Al Kα radiation was 1486.6 eV. The surface morphology of CS was observed under a scanning electron microscope (SEM-EDS, JSM-IT100, Japan JEOL), and its surface element composition was measured by an energy dispersive spectrometer (EDS). The functional group changes of CS were characterized using a Fourier transform infrared spectrometer (FT-IR, Nicolet iS50, Thermo Fisher, USA) (scanning wavelength from 4000 cm^{-1} to 400 cm^{-1}) with KBr tablet technology for spectral analysis. The Raman spectrum of CS was obtained using the Horiba Evolution Raman spectrometer (Paris, France) at excitation wavelength of 532 nm and scanning wavelength range of 100–4000 cm^{-1}. Graphitization features were identified using the ratio (I_D/I_G) of the D (defect) band at about 1350 cm^{-1} to the G (graphite) band at about 1580 cm^{-1} in the Raman spectrum (I_D/I_G).

3. Results And Discussion

3.1. Characterizations of CS

3.1.1 Surface morphology of CS

The SEM images of CS surface under different pyrolysis conditions are shown in Fig. 1. Pyrolysis converts most of the petroleum hydrocarbon pollutants and some soil organic matter into carbonaceous materials that uniformly cover the surface of soil particles, thereby retaining organic carbon that is important to soil health. The surface of the CS sample showed irregular flake particles and spherical particles. The particles are rough and uneven with different sizes and a porous structure. Additional debris was generated on the CS surface.

The EDS analysis of CS_{500-60} is shown in Fig. 1f. The chemical elements with the highest proportions are oxygen, carbon, silicon, aluminum, and calcium. The major solid components of soil are minerals, mainly aluminosilicates; hence, the silicon content of CS was relatively high. After pyrolysis treatment, the content of carbon on the CS surface increased significantly, and that of silicon and oxygen decreased significantly. Carbonization was evident and led to the formation of mineral/carbon composite materials with dark black surface. The significant changes in the content of surface chemical elements inevitably have a significant impact on the surface properties of CS.

3.1.2. Organic element analysis

The contents of C, H, O, N, and S in the CS sample are listed in Table 1. CS had a N content of 0.09–0.17%, C content of 3.11–4.8%, H content of 0.424–0.852%, S content of 0.081–0.111%, and O content of 4.628–5.935%. The the organic elements C, H, O, and N in CS showed a gradually decrease in content with the increase in the final pyrolysis temperature and were further transformed into high calorific value liquid oil and gaseous small molecules, such as H_2, CH_4, and CO, or nitrogen oxide. After remediation, the S content in CS was almost unaffected by pyrolysis temperature and remained at about 0.1%, which was due to the enhanced selective oxidation under the pyrolysis treatment, which further proving that most of the S particles are fixed in CS.

Table 1
Results of analysis of elements in CS. All values in %.

Samples	N	C	H	S	O	H/C	O/C	(O + N)/C
$CS_{400-120}$	0.17	4.8	0.852	0.109	5.935	0.1775	1.236	1.272
CS_{500-30}	0.12	3.27	0.52	0.081	5.478	0.159	1.675	1.712
CS_{500-60}	0.09	3.12	0.487	0.106	5.677	0.156	1.820	1.848
$CS_{500-120}$	0.1	3.11	0.464	0.111	5.848	0.149	1.880	1.913
$CS_{600-120}$	0.09	3.27	0.424	0.107	4.628	0.130	1.415	1.443

(H/C: atomic ratio of hydrogen to carbon; O/C: atomic ratio of oxygen to carbon; (N + O)/C: atomic ratio of the sum of nitrogen and oxygen to carbon)

The C and H contents of each CS were low, indicating that pyrolysis caused the splitting decomposition of the heavy components in PCS. Hydrogen to carbon ratio (H/C) is one of the indicators reflecting the chemical composition of pyrolysis products. The H/C atomic ratio gradually decreased with the increase in temperature, and this phenomenon is related to the cracking (condensation, dehydrogenation, and deoxygenation) reactions of hydrocarbons in PCS (Yan et al. 2009). Hydrogen loss caused by pyrolysis leads to an increase in the ring structure (Vidonish et al. 2016a). The carbon in the aromatized CS is thermally stable, not easily degradable, insoluble in water, and environmentally safe (Liu et al. 2016; Sun et al. 2013). High aromaticity is also conducive to the strong π-π bond interactions between CS and aromatic pollutants (such as AN). O/C and (O + N)/C can reflect the polarity of CS samples (Yuan et al. 2013). High O/C and (O + N)/C indicate high polarity and low hydrophobicity. With the increase in pyrolysis temperature, the O/C and (O + N)/C atomic ratios of CS samples increased first and then decreased. With the increase in retention time at the same temperature, the O/C and (O + N)/C atomic ratios of CS samples showed an upward trend.

3.2. PCS remediation by pyrolysis

3.2.1. TPH removal efficiency

The harmlessness of PCS is crucial for subsequent resource utilization. Therefore, the environmental risks of CS must be investigated. In general, high pyrolysis temperature or residence time improves the removal rate of pollutants, but also leads to high energy consumption and destruction of soil properties. Therefore, Therefore, the determination of PCS pyrolysis parameters must balance the need for pollutant removal and soil function maintenance. The effect of pyrolysis temperature and retention time on the residual TPH concentration in CS is shown in Fig. 2. As displayed in Fig. 2a, the TPH removal rate increased with the pyrolysis temperature. At a pyrolysis temperature of 300°C, the degradation rate of TPH was only 63.01%, during which light hydrocarbon desorption mainly occurred (Vidonish et al. 2018). When the temperature was increased from 300°C to 500°C, the TPH removal rate was as high as 98.89%.

Heavy hydrocarbons (including polycyclic aromatic hydrocarbons) undergo pyrolysis in this stage, and through the cracking, polymerization and aromatization of heavy hydrocarbons, hydrogen and C1-C4 hydrocarbons are released to form non-toxic and stable graphitized carbon (Meng et al. 2003). Further increase in the pyrolysis temperature did not significantly change the TPH removal rate. The effect of retention time on TPH removal rate at 500°C pyrolysis temperature is shown in Fig. 2b. The retention time had no significant effect on the removal rate of TPH. When the pyrolysis temperature was 500°C and the retention time was 60 min, the removal rate of TPH was 98.96% and the residual TPH content in CS was 2857 $mg{\cdot}kg^{-1}$, which is far lower than the second type land control standard value (5000 $mg{\cdot}kg^{-1}$) in the "Soil Environmental Quality Construction Land Soil Pollution Risk Control Standard (GB36600)-2018."

3.2.2. TOC and acute toxicity of CS extracts

The TOC content of extracts was used to reflect the environmental risk of dissolved organic matter in PCS and CS. The effect of pyrolysis temperature on TOC content is shown in Fig. 2c. The TOC content in the PCS extracts was 37.46 $mg{\cdot}L^{-1}$, which was due to the presence of a large amount of TPH in the soil. With the increase in pyrolysis temperature, the TOC content in the CS extracts showed a downward trend and reached the lowest value of 8.34 $mg{\cdot}L^{-1}$ at 600°C. Therefore, the risk of CS extracts was extremely small because a large amount of organic matter in PCS volatilized due to the increase in temperature, leading to the rapid reduction in the content of residual dissolved organic matter. When the pyrolysis temperature is low, organic matter will form dissolved carbon or dissolved organic matter due to incomplete pyrolysis and soft deformable carbon generation, and the prepared CS may exhibit pore deformation (Wang et al. 2017a). As a result, the organic matter easily leaches, and the content of TOC in the extracts becomes relatively high. With the increase in pyrolysis temperature, a large amount of insoluble "char" was produced by pyrolysis, and the organic matter and residual petroleum hydrocarbons in the soil gradually transform into a stable graphite structure. In this work, when the pyrolysis temperature was increased to 500°C, the TOC content in the CS extracts was 10.29 $mg{\cdot}L^{-1}$.

The effect of pyrolysis temperature on the acute toxicity of PCS and CS extracts is shown in Fig. 2c. When the pyrolysis temperature was in the range of 300°C to 500°C, the CS extracts remained safe and non-toxic. With the continuous increase in pyrolysis temperature, the acute toxicity of the CS extracts increased rapidly. When the temperature was raised to 600°C and 700°C, the CS extracts became toxic and severely toxic, respectively. The main reasons may be that high pyrolysis temperature can promote the carbonization of organic matter and increase the degree of graphitization; however, some petroleum hydrocarbon compounds may decompose and produce dissolved toxic substances, resulting in the high ecological risk of CS.

At 500°C pyrolysis temperature, the impact of different retention time (15, 30, 45, 60, 90, and 120 min) on water-soluble matter removal and its biological toxicity is shown in Fig. 2d. The results showed that retention time had no significant effect on the TOC content and acute toxicity of CS extracts. Considering the effects of pyrolysis temperature and retention time on the TPH removal rate of PCS as well as the

TOC content and acute toxicity of PCS extracts, the treatment with pyrolysis temperature of 500°C and retention time of 60 min may yield excellent remediation efficiency.

3.3. AN degradation by CS/PS

3.3.1 Influence of PS and CS dosages

At CS dosage of 5 g·L^{-1}, the effect of PS dosage on the AN removal rate is shown in Fig. 3a. After 5 g·L^{-1} CS_{500-60} was added to the AN solution to react for 6 h, the AN removal rate was 4.52%, indicating that the adsorption and removal capacity of CS itself for AN was almost negligible. When the PS dosage was 1 g·L^{-1}, 73.87% of AN can be removed within 6 h. When the PS dosage was increased to 3 g·L^{-1}, 95.59% of AN can be removed. However, further increase in the PS dosage no longer exhibited a promoting effect on the AN removal rate.

The PS dosage of 3 g·L^{-1} was selected for the subsequent experiment, and the effect of CS dosage on AN removal rate is shown in Fig. 3b. The AN removal rate was 51.23% without CS, indicating that PS can remove AN by direct oxidation. When 2 and 3 g·L^{-1} of CS was added, the AN removal rate increased to 94.77% and 96.09%, respectively. Further increase in CS dosage no longer promoted AN degradation. This is because the addition of excess CS will cause the catalyst particles to agglomerate. As a result, active site are not fully utilized. Therefore, the optimal amount of catalyst CS is 3 g·L^{-1}.

3.3.2 Kinetics of CS-catalyzed PS degradation of AN

The effect of reaction time on AN removal is shown in Fig. 4a. In PS and CS/PS treatments, the AN removal rate increased with the reaction time. The AN removal rate increased rapidly in the first 120 min and then gradually slowed down.

The pseudo first-order model was used to fit the degradation process of AN under different treatments as follows:

$$\ln\left(\frac{C_t}{C_0}\right) = -K_{obs}t\,, \tag{2}$$

$$t_{(\frac{1}{2})} = \frac{\ln 2}{K_{obs}}\,, \tag{3}$$

where C_0 is the initial concentration of AN (mg·L^{-1}), C_t is the concentration of AN (mg·L^{-1}) at a specified time, k_{obs} is the rate constant of AN degradation (min^{-1}), t is time (min), $t_{(1/2)}$ is the half-life (min).

The degradation kinetics of AN is shown in Fig. 4b, and the obtained rate constant (k_{obs}) and half-life ($t_{1/2}$) are shown in Table 2. The reaction rate constant (k_{obs}) of the CS/PS system (0.00858 min^{-1}) is 5.1 times higher than that of the PS system (0.00168 min^{-1}). The $t_{1/2}$ of PS alone treatment was 411.771 min, which was shortened to 80.781 min upon CS addition. Therefore, adding CS as a PS activator significantly increases the AN removal rate, greatly increases the reaction rate, and shortens the reaction time.

Table 2
Quasi-first order reaction kinetic model parameters of AN under different catalytic systems.

Reactant ($3g·L^{-1}$)	$K_{obs}(min^{-1})$	R^2	$t_{1/2}$(min)
PS	0.001683333	0.84071	411.771
PS + CS	0.008580555	0.99234	80.781

3.4. Activation mechanism of CS on PS

3.4.1 Active substance identification

SO_4^{-}· and ·OH are usually the main active substance involved in PS-related advanced oxidation process (AOP) and can effectively destroy organic pollutants (Tsitonaki et al. 2010). However, non-radical oxidation pathways have also been reported in AOP. In these pathways, organic matter is removed through oxidation dominated by $^1O_2$, and the hole interaction between PS and organic matter is mediated by a catalyst. In this study, excessive free radical scavengers (MEOH, IPA, TBA, CF, FA, and EDTA) were added in batch experiments to clarify the main active substances in the CS/PS system for AN degradation (Wang et al. 2019; Bower and Anastasio 2013; Pan et al. 2018).

After different scavengers were added, AN removal was inhibited, and the inhibitory effect varied with the type of scavenger (Fig. 5). Under the action of IPA, TBA, CF, and MEOH, the pure free radical system was terminated, but the removal of AN was not inhibited. This finding indicated that free radicals contributed less to PS activation. On the contrary, the AN degradation in CS/PS system with EDTA addition was completely different, indicating that CS mainly activated PS through non-radical pathways. After 6 h of reaction in the presence of 10 $g·L^{-1}$ of EDTA and FA, the AN removal rate was greatly reduced from the initial 96.09–41.02% and 92.84%, respectively. By contrast, after IPA, TBA, CF, and MEOH (10 $g·L^{-1}$) addition, the AN removal rate remained above 96%. The extremely low AN removal rate in the presence of EDTA indicated that holes are the dominant active species for AN degradation in CS-activated PS system, and these holes can be significantly quenched by EDTA. Carbon-generated holes have similar active sites to ultrasonic and photo-generated holes, which may be responsible for the accelerated degradation of AN

(Velo-Gala et al. 2017). FA also has a certain inhibitory effect on AN degradation by CS/PS, indicating that $^1O_2$ may also be one of the active species.

The above test results show that non-radical pathways play an important role in the CS-activated PS system, and CS-mediated hole generation is the main non-radical pathway. Owing to their low electrochemical impedance and good conductivity, carbon materials can directly transfer electrons and produce some active substances as electronic media to activate PS; this ability is related to electron holes, porous structure, and charge transfer complexes (Gao et al. 2022). Studies have shown that carbonyl groups (C = O) and organics in CS can form singlet oxygen precursors, leading to the formation of $^1O_2$ (Fang et al. 2017). The graphitized defect structure of carbon materials provides active centers for electron holes and a strong electron-accepting ability for aromatic pollutants through the conjugated π-electron system. The aromatic structure and graphitized structure of carbon materials are the media of the electronic shuttle (Ghanbari and Moradi 2017). In this reaction system, CS is used as the transmission medium. $S_2O_8^{2-}$ is adsorbed on the surface of the positively charged CS and then reduced by electron donor, coupled with the generation of the holes (Wu et al. 2018). The holes may accelerate electron transfer and facilitated the oxidative degradation of AN.

3.4.2 Raman and FT-IR analysis

Raman spectroscopy was performed to determine the characteristics of the carbon structure of CS under different pyrolysis conditions (Fig. 6a). Two different peaks were observed at 1350 and 1600 cm^{-1} and were named as D and G bands, respectively. D band represents the amorphous carbon structure in carbon materials, and G band represents the vibration of sp^2 hybrid carbon atoms in graphitized carbon (Yuan et al. 2013). The intensity ratio of peak D to peak G (I_D/I_G) was used to evaluate the crystal defect degree and graphitization degree of the CS sample. The results showed that CS_{500-60} had the highest graphitization degree. After the temperature and retention time were increased, the I_D/I_G values of $CS_{500-120}$ and $CS_{600-120}$ dropped to 0.622 and 0.687, respectively. This phenomenon occurred because when the pyrolysis temperature exceeded 500°C, the graphitized structure of CS was destroyed. This finding is consistent with the previous elemental analysis results.

FTIR was used to determine the functional groups of CS samples under different pyrolysis conditions as shown in Fig. 6b. The results showed that the CS samples have a wide range of absorption peaks at 3730, 3420, 2920, 2850, 1630, 1430, 1020, 775, and 462 cm^{-1}. The broad spectrum between 3730 and 3420 cm^{-1} was due to -OH stretching, thus indicating the presence of alcohol and phenol functional groups. However, as the pyrolysis temperature increases, the adsorption band of -OH gradually weakens, which indicates that the pyrolysis produces secondary cracking and dehydroxylation reactions to form a graphitic structure (Wang and Rinaldi 2013). The absorption peaks at 2850 and 2920 cm^{-1} were attributed to the symmetric and asymmetric C-H stretching vibrations of petroleum hydrocarbons (Li et al. 2018), respectively. These two peaks were weakened when the pyrolysis temperature was set to 400°C and almost completely disappeared at 500°C, implying the complete removal of petroleum hydrocarbons.

The extremely weak absorption peak at 1630 cm^{-1} represented the C = O group, which is the active site for generating $^1O_2$ (Zhou et al. 2015). In addition, the absorption peak at 1430 cm^{-1} corresponded to the stretching vibration of the C-H bond in the aliphatic structure, the asymmetric and symmetric C-H bending of the methyl group, and the stretching vibration of = CH_2. The broadband near 1020 cm^{-1} represented the presence of ether (C-O stretch) (Zhao et al. 2016). The band at 775 cm^{-1} corresponded to the skeleton vibration of the aromatic structure (Zhang et al. 2016). The adsorption peak at 462 cm^{-1} was related to the Si-O stretching vibration, which corresponded to the silica and silicate of CS (Abrego et al. 2009).

According to FTIR analysis, CS contained a large amount of ethers, alcohols, alkanes, and aromatic hydrocarbons. With the increase of pyrolysis temperature and the prolongation of retention time, the unstable oxygen-containing functional groups gradually decreased, and the aromatic structure gradually increased (Zhao et al. 2016). Low adsorption capacity of CS in this study may be related to the loss of oxygen-containing functional groups on the surface and the strong hydrophobicity caused by the graphitization of C due to the deoxygenation and dehydrogenation of CS with the increase in pyrolysis temperature (Liu et al. 2020). This finding also verified that CS did not show adsorption in the AN degradation batch experiment. The graphitized carbon produced by pyrolysis usually forms a defect structure, that is, a large number of holes are generated, which can accelerate the electron transfer in the oxidation reaction system, thereby improving the oxidative degradation efficiency and rate of organic pollutants (Huang et al. 2021). The oxygen-containing functional group can often also act as a persulfate activator, but it also occupies defect sites in graphitic carbon, thereby inhibiting the activation of persulfate by holes. Therefore, the pyrolysis temperature and retention time have a significant effect on the degree of graphitization of organic carbon in PCS, which in turn affects the types of PS-activating species in CS and their activation mechanism. The CS has a higher degree of graphitization in this study, so holes dominate the PS activation.

3.4.3 XPS analysis

The element composition and surface chemical state of the CS_{500-60} sample were studied by XPS (Fig. 7). The full view of the XPS spectrum (Fig. 7a) shows that carbon and oxygen are the main chemical components on the surface of the material, which is consistent with EDS. Small amounts of nitrogen, chlorine and silicon, and trace iron elements, apparently come from various inorganic soil minerals. The lower carbon content is closely related to the removal of petroleum pollutants, which leads to the increase of O and Si elements in the soil surface (Vidonish et al. 2018). As shown in Fig. 7b, the C1s spectrum was divided into five peaks, namely, graphic C (284.8 eV), C-C (285.69 eV), C = O (286.8 eV), -COOH (290 eV), and π-π* (293.88 eV) (Liu et al. 2020; Gao et al. 2019; Qian et al. 2014; Okpalugo et al. 2005). Carbon configuration is an important factor that controls the catalytic performance of PS activation (Song et al. 2022). Graphitic carbon is carbon in the configuration SP^2 hybrid. Comparison of sp^3C-C and sp^2C = C peaks confirmed the coexistence of graphite and amorphous carbon in the CS sample. The graphitic carbon can be used as a fast electron transport medium, and highly conducive to non-radical pathways (Song et al. 2022). Graphitic carbon has strong catalytic activity in PS-AOPS, and high CS graphitic

carbon content can be obtained by high-temperature pyrolysis of heavy hydrocarbons in PCS (Kang et al. 2020; Wu et al. 2022). Graphitic carbon makes the adjacent carbon atoms positively charged, and $S_2O_8^{2-}$ is adsorbed on the charged carbon atoms and reduced by electron-donating groups. CS also had defects and certain oxygen-containing functional groups, which are conducive to PS activation. The aromatic structure can determine the carbon fixation capacity of CS through π-π; hence, the TOC content of the CS extracts was low when pyrolyzed at 500°C (McBeath et al. 2015).

As shown in Fig. 7c, the O1s region was convolved as four peaks at 530.33, 531.60, 532.45 and 533.10 eV due to Si-O (Gao et al. 2019), C = O (Shen et al. 2022), organic C-O and COOH (Wang et al. 2017b; Liu et al. 2021), respectively. PCS contains a large amount of C-O bonds, while a small amount of organic C-O peak was observed after pyrolysis, indicating that the oxygen-rich organic matter was carbonized during the process. This finding further confirmed the existence of oxygen-rich organic matter converted into stable graphitic carbon by thermal polycondensation and cyclization (Kou et al. 2021; Zhao et al. 2016). The Si-O bond represents the SiO_2 in the solid component of the soil. As shown in Fig. 7d, the Si1s region was convolved as a peakat 103.23 eV, representing Si-O. It shows that oil pollution does not change the mineral characteristics of surface soil particles.

3.5 Recycling of CS

Reusability and stability are the key characteristics of catalysts for wastewater treatment. The results of the recycling experiment are shown in Fig. 8. In the first two operating cycles, the removal rates of AN and TOC were relatively stable at above 80% and 65%, respectively. However, starting from the third cycle, the catalytic ability of CS began to gradually decrease, and the removal rates of AN and TOC were 74.01% and 59.83%, respectively. After five regeneration cycles, the removal rates of AN and TOC dropped to 53.73% and 51.54%, respectively. The gradually decrease in CS activation efficiency may be due to the degradation products and intermediates occupying the pores of the CS surface, covering the active sites, and blocking the adsorption and activation of CS on PS (Wang and Wang 2019).

4. Conclusions

In this study, the harmlessness of PCS and the feasibility of its simultaneous resource utilization and recycling to produce CS by oxygen-limited pyrolysis was studied. The results showed that at pyrolysis temperature of 500°C and retention time of 60 min, the majority TPH was removed, and the extracts show extremely low concentration of dissolved TOC and no acute toxicity. CS showed high PS activation performance for AN degradation. When the dosages of CS and PS were 3 $g \cdot L^{-1}$, the AN removal rate reached 96.09%. CS maintained a certain PS activation performance after five recycling times. Active species quenching experiments revealed that the non-radical pathways played a dominant role in CS-activated PS system for oxidation, and the hole was the main active species, followed by $^1O_2$. This study

provides an innovative approach for the simultaneous high-efficiency remediation and high-value resource utilization for PCS and thus has a good prospect for large-scale application.

Declarations

Author contribution Yaping Liao: Methodology, Data curation, Formal analysis, Writing - Original Draft. Hang Gao: Data curation, Validation. Mingxin Wang: Conceptualization, Writing - Review & Editing, Funding acquisition. Jinjuan Xue: Resources, Project administration. Meng Yao: Validation.

Funding This work was supported by the National Natural Science Foundation of China under grants (No.41772240), and the Key Research and Development program of Jiangsu Province (BE2021237).

Material and Data availability The Material and data sets supporting the results of this article are included within the article.

Competing of interest The authors declare they have no competing interests.

Ethical Approval and Consent to participate Not applicable.

Consent to publication All authors would like to have it considered exclusively for publication in *Environmental Science and Pollution Research*.

References

1. Abrego J, Arauzo J, Luis SJ, Gonzalo A, Cordero T, Rodriguez-Mirasol J (2009) Structural Changes of Sewage Sludge Char during Fixed-Bed Pyrolysis. Ind Eng Chem Res 48: 3211-3221. https://doi.org/10.1021/ie801366t.
2. Bower JP, Anastasio C (2013) Measuring a 10,000-fold enhancement of singlet molecular oxygen ($^1O_2$*) concentration on illuminated ice relative to the corresponding liquid solution. Atmos Environ 75: 188-195. https://doi.org/10.1016/j.atmosenv.2013.04.054.
3. Fang GD, Liu C, Wang YJ, Dionysiou DD, Zhou DM (2017) Photogeneration of reactive oxygen species from biochar suspension for diethyl phthalate degradation. Appl Catal B-Environ 214: 34-45. https://doi.org/10.1016/j.apcatb.2017.05.036
4. Gao RT, Liu Y, Liu BY, Xu ZM (2019) Novel utilization of pyrolysis products produced from waste printed circuit boards: catalytic cracking and synthesis of graphite carbon. J Clean Prod 236: 117662. https://doi.org/10.1016/j.jclepro.2019.117662.
5. Gao Y, Wang Q, Ji GZ, Li AM (2022) Degradation of antibiotic pollutants by persulfate activated with various carbon materials. Chem Eng J 429: 132387. https://doi.org/10.1016/j.cej.2021.132387.
6. Gao Y, Zygourakis K (2019) Kinetic Study of the Pyrolytic Treatment of Petroleum Contaminated Soils. Ind Eng Chem Res 58: 10829-10843. https://doi.org/10.1021/acs.iecr.9b01494.

7. Ghanbari F, Moradi M (2017) Application of peroxymonosulfate and its activation methods for degradation of environmental organic pollutants: Review. Chem Eng J 310: 41-62. https://doi.org/10.1016/j.cej.2016.10.064.
8. Huang WQ, Xiao S, Zhong H, Yan M, Yang X (2021) Activation of persulfates by carbonaceous materials: A review. Chem Eng J 418: 129297. https://doi.org/10.1016/j.cej.2021.129297.
9. Kang CU, Kim DH, Khan MA, Kumar R, Ji SE, Choi KW, Paeng KJ, Park S, Jeon BH (2020) Pyrolytic remediation of crude oil-contaminated soil. Sci Total Environ 713: 136498. https://doi.org/10.1016/j.scitotenv.2020.136498.
10. Kim Y, Oh JI, Lee SS, Lee KH, Lee J, Kwon EE (2019) Decontamination of petroleum-contaminated soil via pyrolysis under carbon dioxide atmosphere. J Clean Prod 236: 117724. https://doi.org/10.1016/j.jclepro.2019.117724..
11. Kohantorabi M, Moussavi G, Giannakis S (2021) A review of the innovations in metal- and carbon-based catalysts explored for heterogeneous peroxymonosulfate (PMS) activation, with focus on radical vs . non-radical degradation pathways of organic contaminants. Chem Eng J 411: 127957. https://doi.org/10.1016/j.cej.2020.127957.
12. Kou LD, Wang J, Zhao L, Jiang K, Xu XX (2021) Coupling of $KMnO_4$-assisted sludge dewatering and pyrolysis to prepare Mn,Fe-codoped biochar catalysts for peroxymonosulfate-induced elimination of phenolic pollutants. Chem Eng J 411: 128459. https://doi.org/ 10.1016/j.cej.2021.128459.
13. Lassalle G, Gassend V, Michaudel G, Hedacq R, Weber C, Jennet C, Souquet P, Credoz A (2021) A multicriteria approach for assessing the recovery of soil functions following high-temperature remediation of hydrocarbons. Sci Total Environ 775: 145891. https://doi.org/ 10.1016/j.scitotenv.2021.145891.
14. Li DC, Xu WF, Mu Y, Yu HQ, Jiang H, Crittenden JC (2018) Remediation of Petroleum-Contaminated Soil and Simultaneous Recovery of Oil by Fast Pyrolysis. Environ Sci Technol 52: 5330-5338.https://doi.org/10.1021/acs.est.7b03899.
15. Li Z, Ronen Z, Gelman F, Crouvi O, Arye G, Rosenzweig R (2021) Reclamation of oil-induced soil hydrophobicity in the hyper-arid Evrona Nature Reserve, southern Israel. Pedosphere 31: 892-902. https://doi.org/ 10.1016/S1002-0160(21)60031-0.
16. Liu XQ, Ding HS, Wang YY, Liu WJ, Jiang H (2016) Pyrolytic Temperature Dependent and Ash Catalyzed Formation of Sludge Char with Ultra-High Adsorption to 1-Naphthol. Environ Sci Technol 50: 2602-2609. https://doi.org/10.1021/acs.est.5b04536.
17. Liu YQ, Li XD, Zhang WW, Dou JF, Zhang Q, Ma FJ, Gu QB (2021) Effect and mechanisms of red mud catalyst on pyrolysis remediation of heavy hydrocarbons in weathered petroleum-contaminated soil. J Environ Chem Eng 9: 106090. https://doi.org/10.1016/j.jece.2021.106090.
18. Liu YQ, Zhang Q, Wu B, Li XD, Ma FJ, Li FS, Gu QB (2020) Hematite-facilitated pyrolysis: An innovative method for remediating soils contaminated with heavy hydrocarbons. J Hazard Mater 383: 121165. https://doi.org/10.1016/j.jhazmat.2019.121165.

19. Lyu C, He D, Chang YM, Zhang QH, Wen F, Wang XS (2019) Cobalt oxyhydroxide as an efficient heterogeneous catalyst of peroxymonosulfate activation for oil-contaminated soil remediation. Sci Total Environ 680: 61-69. https://doi.org/10.1016/j.scitotenv.2019.04.324.
20. McAlexander BL, Krembs FJ, Cardenosa Mendoza M (2015) Treatability Testing for Weathered Hydrocarbons in Soils: Bioremediation, Soil Washing, Chemical Oxidation, and Thermal Desorption. Soil Sediment Contam 24: 882-897. https://doi.org/ 10.1080/15320383.2015.1064088.
21. McBeath AV, Wurster CM, Bird MI (2015) Influence of feedstock properties and pyrolysis conditions on biochar carbon stability as determined by hydrogen pyrolysis. Biomass Bioenerg 73: 155-173. https://doi.org/10.1016/j.biombioe.2014.12.022.
22. Meng XH, Xu CM, Li L, Gao JS (2003) Studies on the kinetics of heavy oil catalytic pyrolysis. Ind Eng Chem Res 42: 6012-6019. https://doi.org/10.1021/ie030433l.
23. Mishra S, Lin ZQ, Pang SM, Zhang YM, Bhatt P, Chen SH (2021) Biosurfactant is a powerful tool for the bioremediation of heavy metals from contaminated soils. J Hazard Mater 418: 126253. https://doi.org/ 10.1016/j.jhazmat.2021.126253.
24. Mustapha NA, Liu H, Ibrahim AO, Huang Y, Liu S (2021) Degradation of aniline in groundwater by persulfate with natural subsurface sediment as the activator. Chem Eng J 417: 128078. https://doi.org/ 10.1016/j.cej.2020.128078.
25. Okpalugo TIT, Papakonstantinou P, Murphy H, McLaughlin J, Brown NMD (2005) High resolution XPS characterization of chemical functionalised MWCNTs and SWCNTs. Carbon 43: 153-161. https://doi.org/10.1016/j.carbon.2004.08.033.
26. Pan Y, Su HR, Zhu YT, Molamahmood FV, Long M (2018) CaO_2 based Fenton-like reaction at neutral pH: Accelerated reduction of ferric species and production of superoxide radicals. Water Res 145: 731-740. https://doi.org/10.1016/j.watres.2018.09.020.
27. Pham VL, Kim DG, Ko SO (2020) Advanced oxidative degradation of acetaminophen by carbon catalysts: Radical vs non-radical pathways. Environ. Res 188: 109767. https://doi.org/10.1016/j.envres.2020.109767.
28. Qian TT, Li DC, Jiang H (2014) Thermochemical Behavior of Tris(2-Butoxyethyl) Phosphate (TBEP) during Co-pyrolysis with Biomass. Environ Sci Technol 48: 10734-10742. https://doi.org/ 10.1021/es502669s.
29. Ren JQ, Song X, Ding D (2020) Sustainable remediation of diesel-contaminated soil by low temperature thermal treatment: Improved energy efficiency and soil reusability. Chemosphere 241: 124952. https://doi.org/10.1016/j.chemosphere.2019.124952.
30. Shen YQ, Zhu K, He DD, Huang J, He HM, Lei LL, Chen WJ (2022) Tetracycline removal via adsorption and metal-free catalysis with 3D macroscopic N-doped porous carbon nanosheets: Non-radical mechanism and degradation pathway. J Environ Sci 111: 351-366. https://doi.org/10.1016/j.jes.2021.04.014.
31. Song G, Qin FZ, Yu JF, Tang L, Pang Y, Zhang C, Wang JJ, Deng LF (2022) Tailoring biochar for persulfate-based environmental catalysis: Impact of biomass feedstocks. J Hazard Mater 424:

127663. https://doi.org/10.1016/j.jhazmat.2021.127663.

32. Song W, Vidonish JE, Kamath R, Yu P, Chu C, Moorthy B, Gao B, Zygourakis K, Alvarez PJJ (2019) Pilot-Scale Pyrolytic Remediation of Crude-Oil-Contaminated Soil in a Continuously-Fed Reactor: Treatment Intensity Trade-Offs. Environ Sci Technol 53: 2045-2053. https://doi.org/10.1021/acs.est.8b05825.
33. Sun K, Kang MJ, Zhang ZY, Jin J, Wang ZY, Pan ZZ, Xu DY, Wu FC, Xing BS (2013) Impact of Deashing Treatment on Biochar Structural Properties and Potential Sorption Mechanisms of Phenanthrene. Environ Sci Technol 47: 11473-11481. https://doi.org/10.1021/es4026744.
34. Tsitonaki A, Petri B, Crimi M, Mosbaek H, Siegrist RL, Bjerg PL (2010) In Situ Chemical Oxidation of Contaminated Soil and Groundwater Using Persulfate: A Review. Crit Rev Env Sci Tec 40: 55-91. https://doi.org/10.1080/10643380802039303.
35. Velo-Gala I, Lopez-Penalver JJ, Sanchez-Polo M, Rivera-Utrilla J (2017) Role of activated carbon surface chemistry in its photocatalytic activity and the generation of oxidant radicals under UV or solar radiation. Appl Catal B-Environ 207: 412-423. https://doi.org/10.1016/j.apcatb.2017.02.028.
36. Vidonish JE, Alvarez PJJ, Zygourakis K (2018) Pyrolytic Remediation of Oil-Contaminated Soils: Reaction Mechanisms, Soil Changes, and Implications for Treated Soil Fertility. Ind Eng Chem Res 57: 3489-3500. https://doi.org/10.1021/acs.iecr.7b04651.
37. Vidonish JE, Zygourakis K, Masiello CA, Gao X, Mathieu J, Alvarez PJJ (2016a) Pyrolytic Treatment and Fertility Enhancement of Soils Contaminated with Heavy Hydrocarbons. Environ Sci Technol 50: 2498-2506. https://doi.org/10.1021/acs.est.5b02620.
38. Vidonish JE, Zygourakis K, Masiello CA, Sabadell G, Alvarez PJJ (2016b) Thermal Treatment of Hydrocarbon-Impacted Soils: A Review of Technology Innovation for Sustainable Remediation. Engineering-Prc 2: 426-437. https://doi.org/ 10.1016/J.ENG.2016.04.005.
39. Wang B, Li YN, Wang L (2019) Metal-free activation of persulfates by corn stalk biochar for the degradation of antibiotic norfloxacin: Activation factors and degradation mechanism. Chemosphere 237: 124454. https://doi.org/10.1016/j.chemosphere.2019.124454.
40. Wang BY, Zhang W, Li H, Fu HY, Qu XL, Zhu DQ (2017a) Micropore clogging by leachable pyrogenic organic carbon: A new perspective on sorption irreversibility and kinetics of hydrophobic organic contaminants to black carbon. Environmental Pollution 220: 1349-1358. https://doi.org/10.1016/j.envpol.2016.10.100.
41. Wang SZ, Wang JL (2019) Activation of peroxymonosulfate by sludge-derived biochar for the degradation of triclosan in water and wastewater. Chem Eng J 356: 350-358. https://doi.org/ 10.1016/j.cej.2018.09.062.
42. Wang XP, Gu L, Zhou P, Zhu NW, Li CX, Tao H, Wen HF, Zhang DF(2017b) Pyrolytic temperature dependent conversion of sewage sludge to carbon catalyst and their performance in persulfate degradation of 2-Naphthol. Chem Eng J 324: 203-215. https://doi.org/10.1016/j.cej.2017.04.101.
43. Wang XY, Rinaldi R (2013) A Route for Lignin and Bio-Oil Conversion: Dehydroxylation of Phenols into Arenes by Catalytic Tandem Reactions. Angew. Chem Int Edit 52: 11499-11503.

https://doi.org/10.1002/anie.201304776.

44. Wu GZ, Coulon F, Yang YW, Li H, Sui H (2013) Combining Solvent Extraction and Bioremediation for Removing Weathered Petroleum from Contaminated Soil. Pedosphere 23: 455-463. https://doi.org/10.1016/S1002-0160(13)60038-7.
45. Wu L, Wu T, Liu ZF, Tang WW, Xiao S, Shao BB, Liang QH, He QY, Pan Y, Zhao CH, Liu Y, Tong SH (2022) Carbon nanotube-based materials for persulfate activation to degrade organic contaminants: Properties, mechanisms and modification insights. J Hazard Mater 431: 128536. https://doi.org/10.1016/j.jhazmat.2022.128536.
46. Wu Y, Guo J, Han YJ, Zhu JY, Zhou LX, Lan YQ (2018) Insights into the mechanism of persulfate activated by rice straw biochar for the degradation of aniline. Chemosphere 200: 373-379. https://doi.org/ 10.1016/j.chemosphere.2018.02.110.
47. Yan SC, Li ZS, Zou ZG (2009) Photodegradation Performance of g-C_3N_4 Fabricated by Directly Heating Melamine. Langmuir 25: 10397-10401. https://doi.org/10.1021/la900923z.
48. Yuan HR, Lu T, Zhao DD, Huang HY, Noriyuki K, Chen Y (2013) Influence of temperature on product distribution and biochar properties by municipal sludge pyrolysis. J Mater Cycles Waste 15: 357-361. https://doi.org/10.1007/s10163-013-0126-9.
49. Zhang RD, Liu N, Lei ZG, Chen BH (2016) Selective Transformation of Various Nitrogen-Containing Exhaust Gases toward N-2 over Zeolite Catalysts. Chem Rev 116: 3658-3721. https://doi.org/10.1021/acs.chemrev.5b00474.
50. Zhao YJ, Feng DD, Zhang Y, Huang YD, Sun SZ (2016) Effect of pyrolysis temperature on char structure and chemical speciation of alkali and alkaline earth metallic species in biochar. Fuel Process Technol 141: 54-60. https://doi.org/10.1016/j.fuproc.2015.06.029.
51. Zhou Y, Jiang J, Gao Y, Ma J, Pang SY, Li J, Lu XT, Yuan LP (2015) Activation of Peroxymonosulfate by Benzoquinone: A Novel Nonradical Oxidation Process. Environ Sci Technol 49: 12941-12950. https://doi.org/10.1021/acs.est.5b03595.

Figures

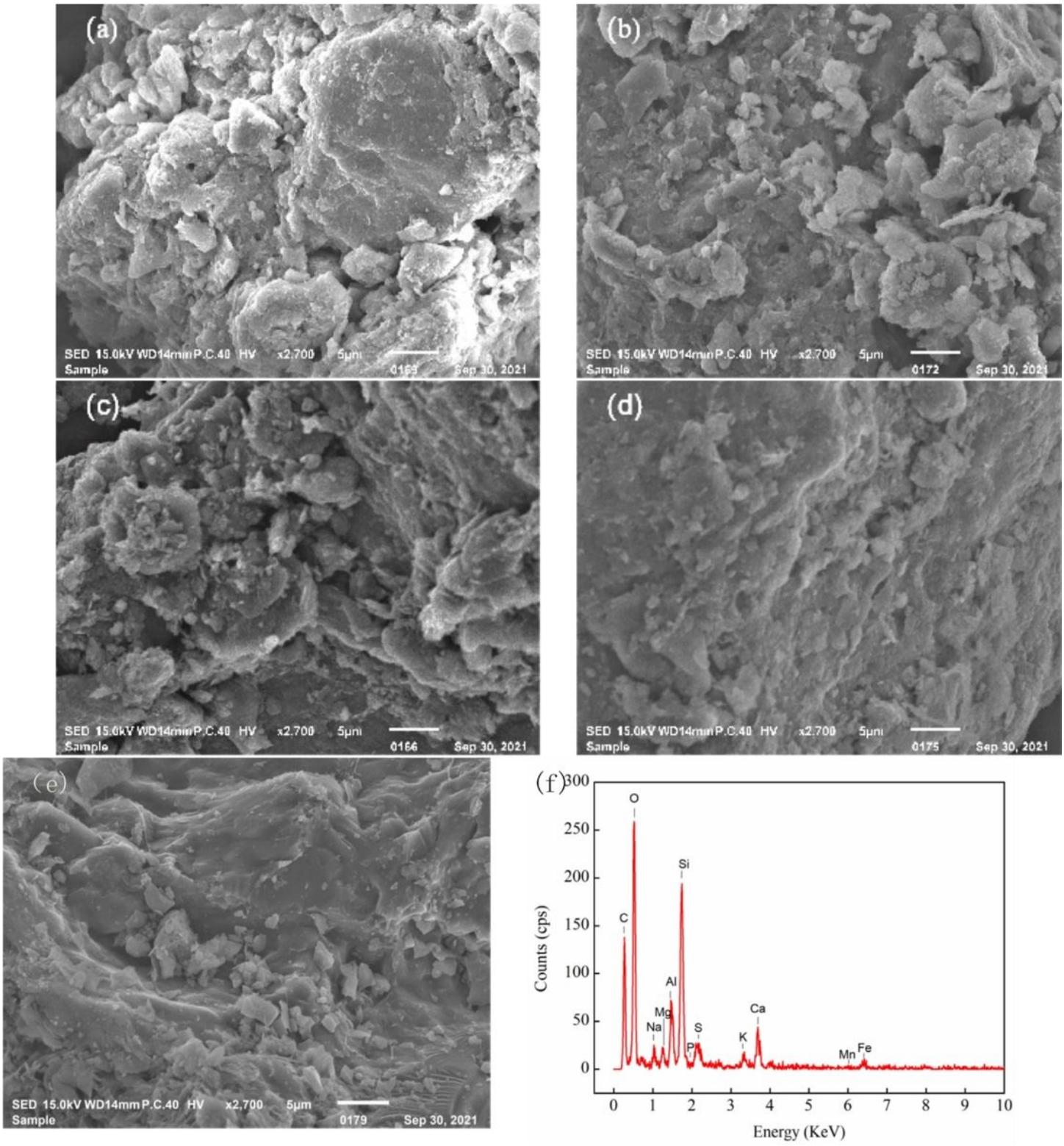

Figure 1

SEM images of (a) $CS_{400\text{-}120}$, (b) $CS_{500\text{-}120}$, (c) $CS_{600\text{-}120}$, (d) $CS_{500\text{-}30}$, and (e) $CS_{500\text{-}60}$; and (f) EDS image of $CS_{500\text{-}60}$.

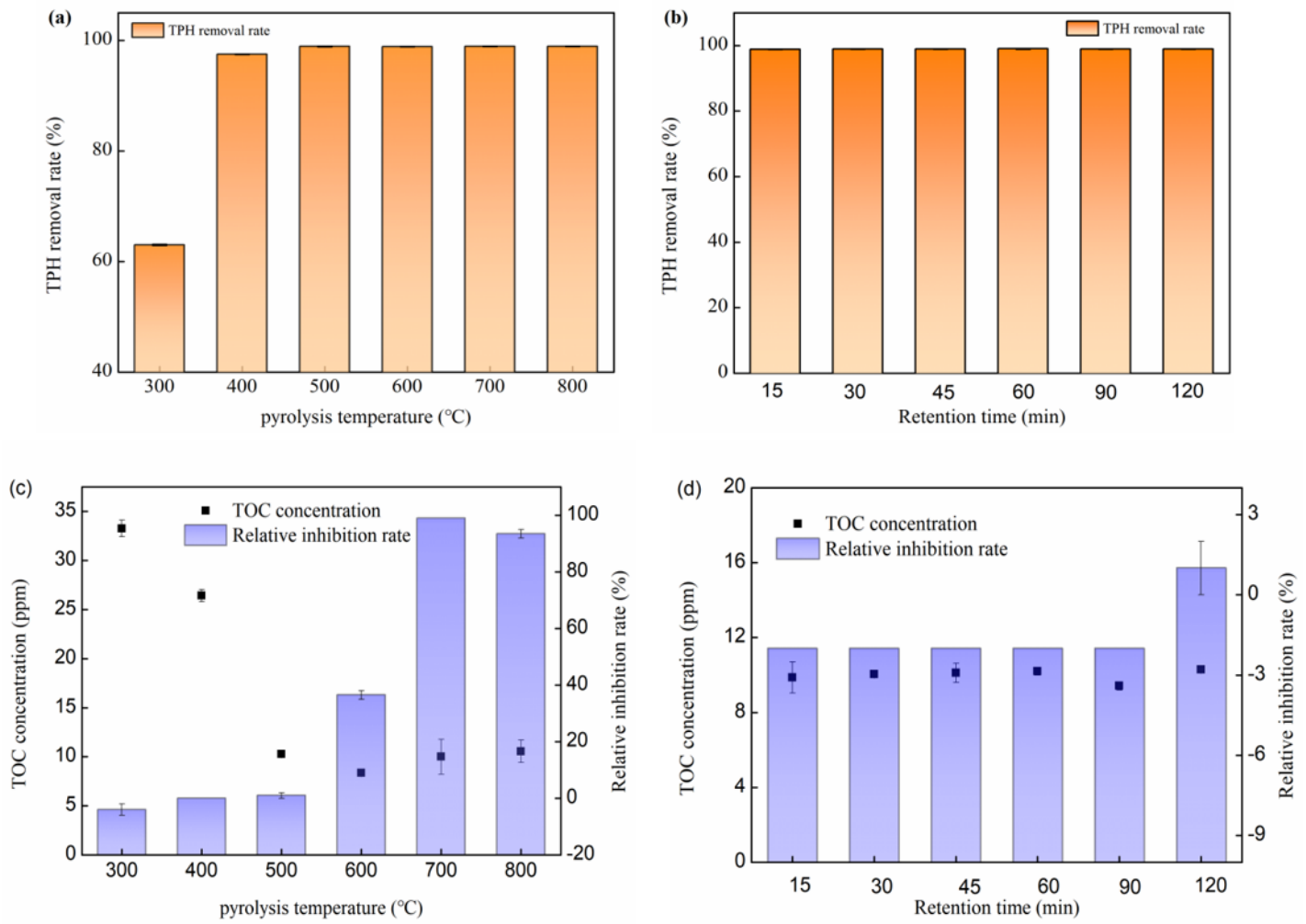

Figure 2

The effects of (a) pyrolysis temperature and (b) retention time on TPH removal rate, (c) pyrolysis temperature and (d) retention time on TOC and acute toxicity of PCS and CS extracts.

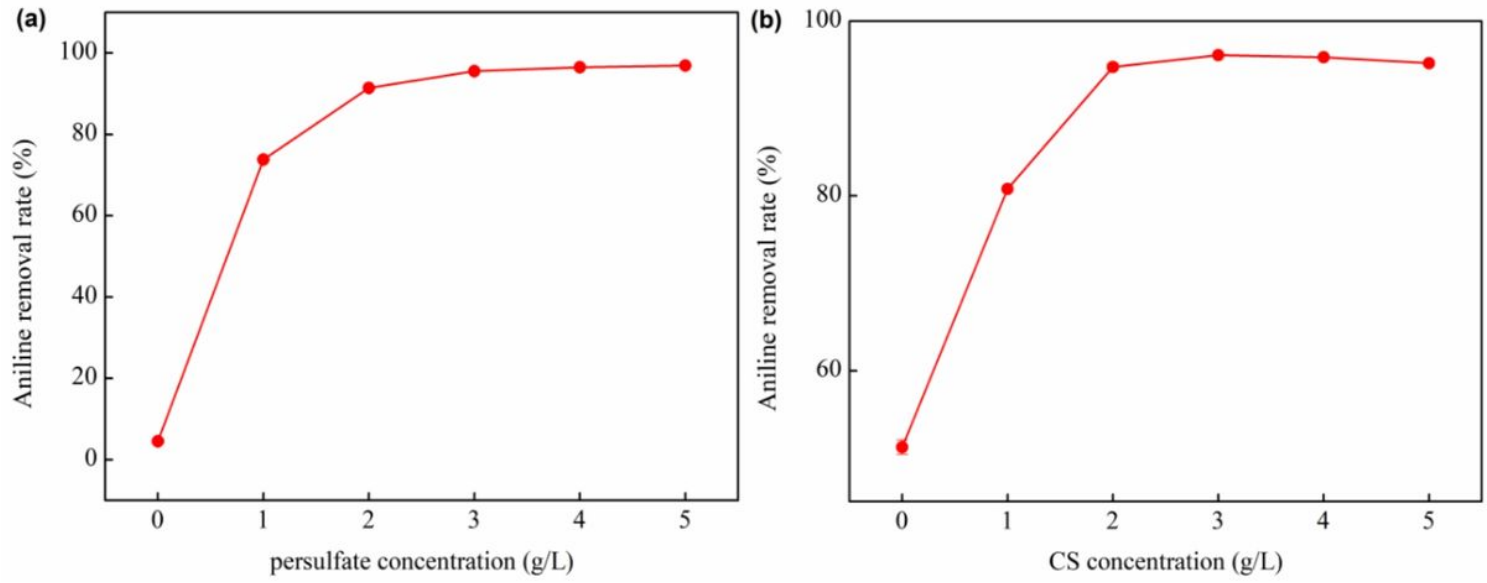

Figure 3

Effect of (a) PS dosage and (b) CS dosage on AN removal rate (pyrolysis temperature = 500 °C, retention time=60min, $[AN]_0$=100 mg·L^{-1}, and reaction time = 6 h).

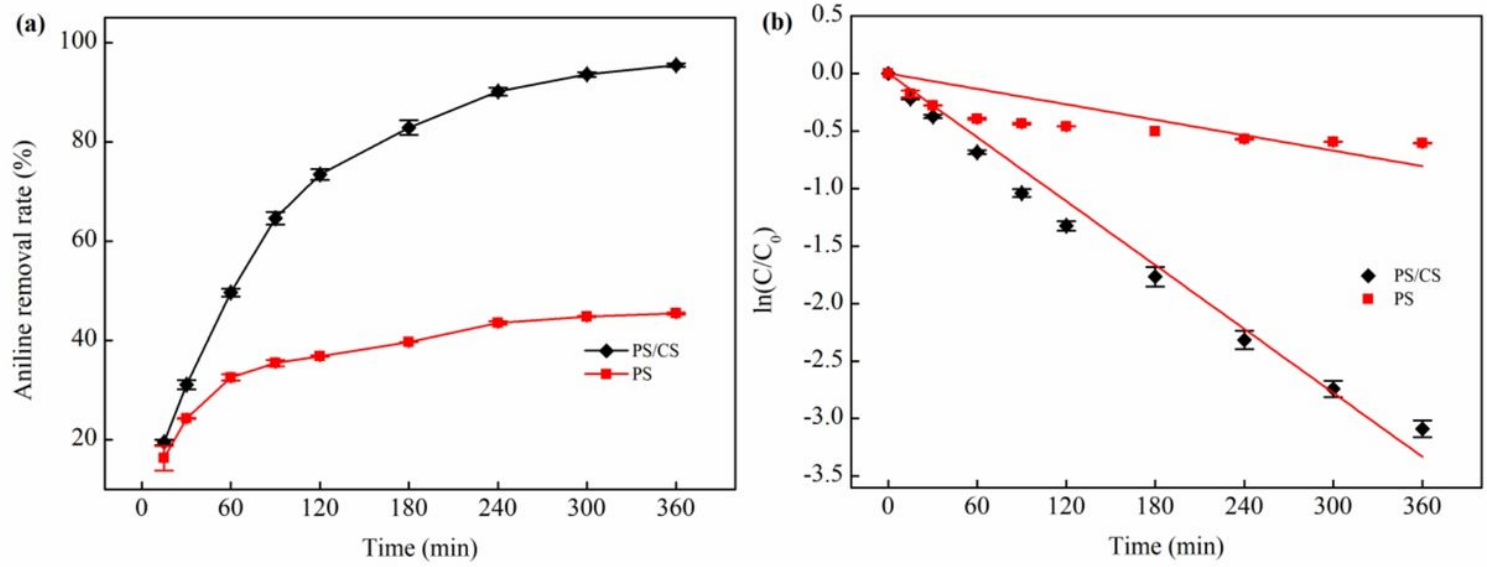

Figure 4

(a) Effect of reaction time on AN degradation. (b) Degradation kinetics of AN in different treatments ($[AN]_0$=100 mg·L^{-1}, $[PS]_0$=3 g·L^{-1}, $[CS]_0$=3 g·L^{-1}).

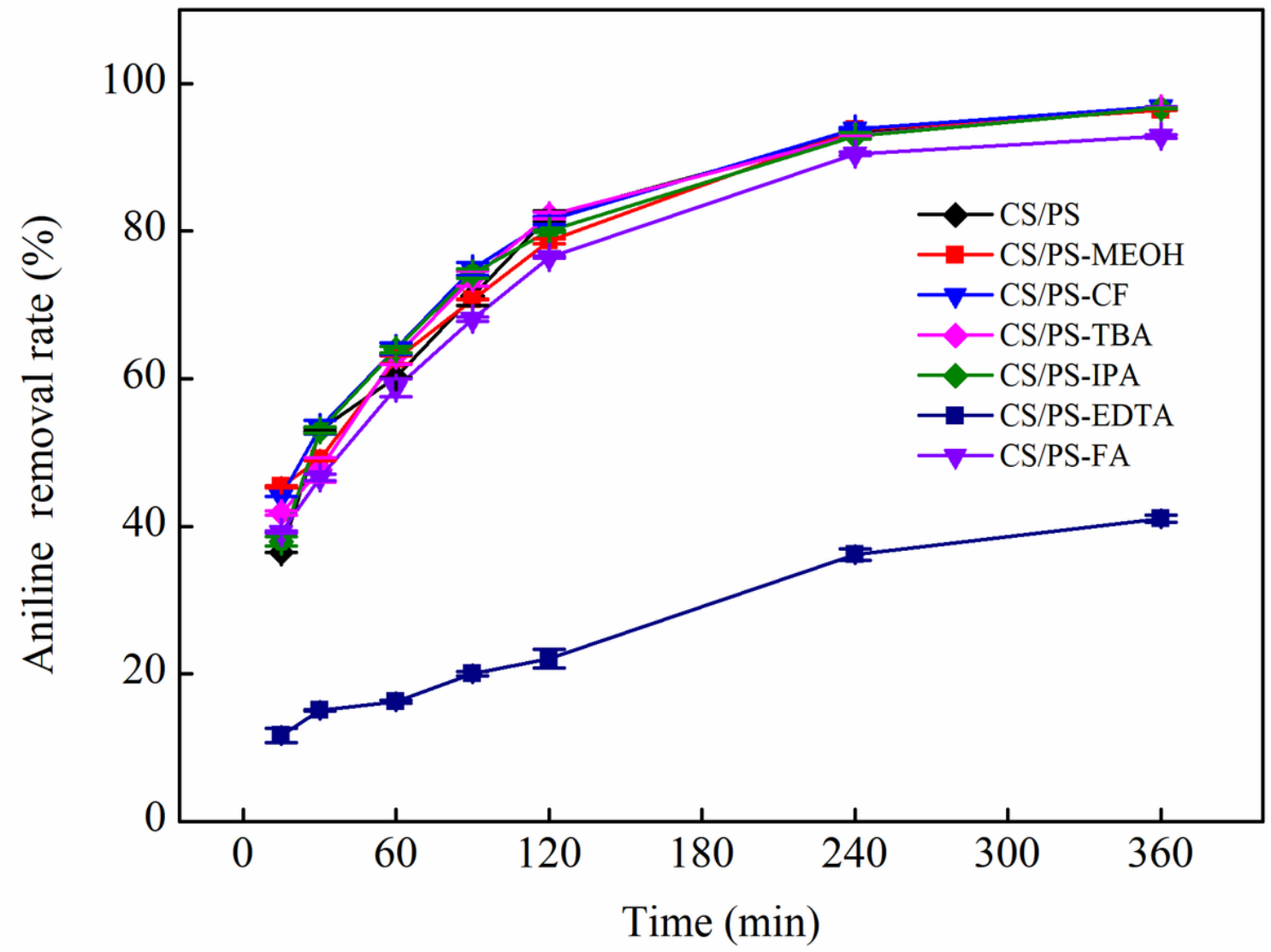

Figure 5

Effect of different scavengers on CS-activated PS system for AN degradation ($[AN]_0$=100 mg·L^{-1}, $[PS]_0$=3 g·L^{-1}, $[CS]_0$=3 g·L^{-1}, $[Quencher]_0$=10 g·L^{-1}, reaction time = 6 h).

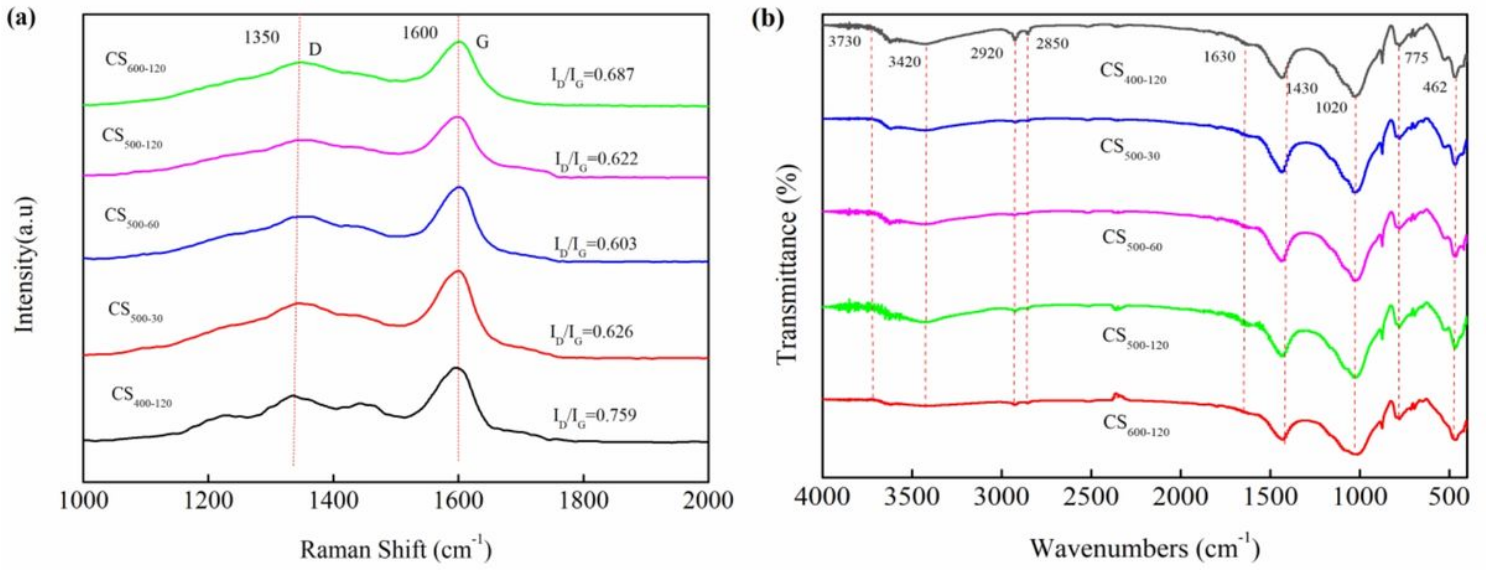

Figure 6

(a) Raman and (b) FT-IR spectra of CS under different pyrolysis conditions.

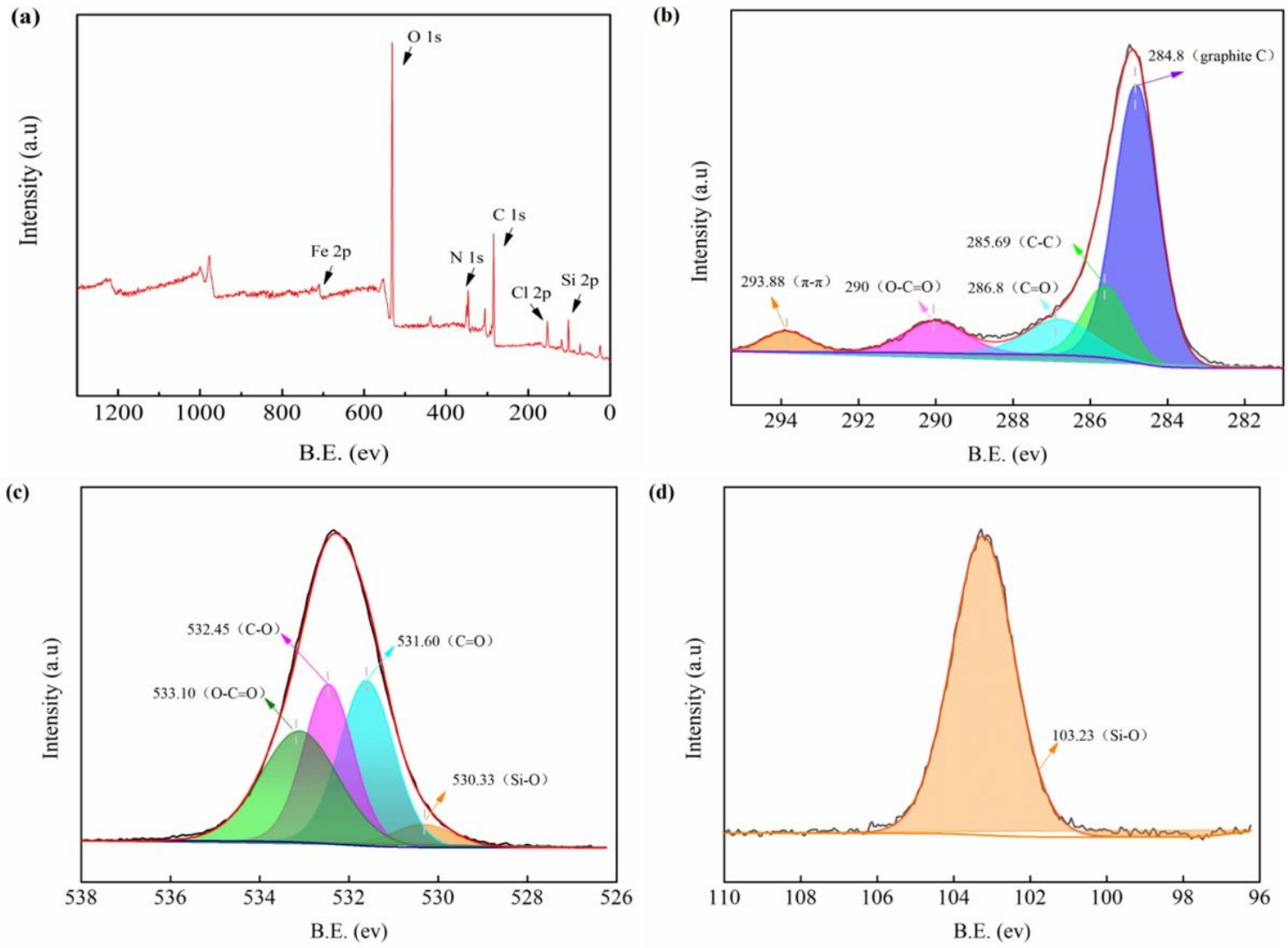

Figure 7

XPS spectrum of $CS_{500\text{-}60}$. (a) $CS_{500\text{-}60}$ Score; (b) C1s atlas; (c) O1s atlas;(d) Si1s atlas.

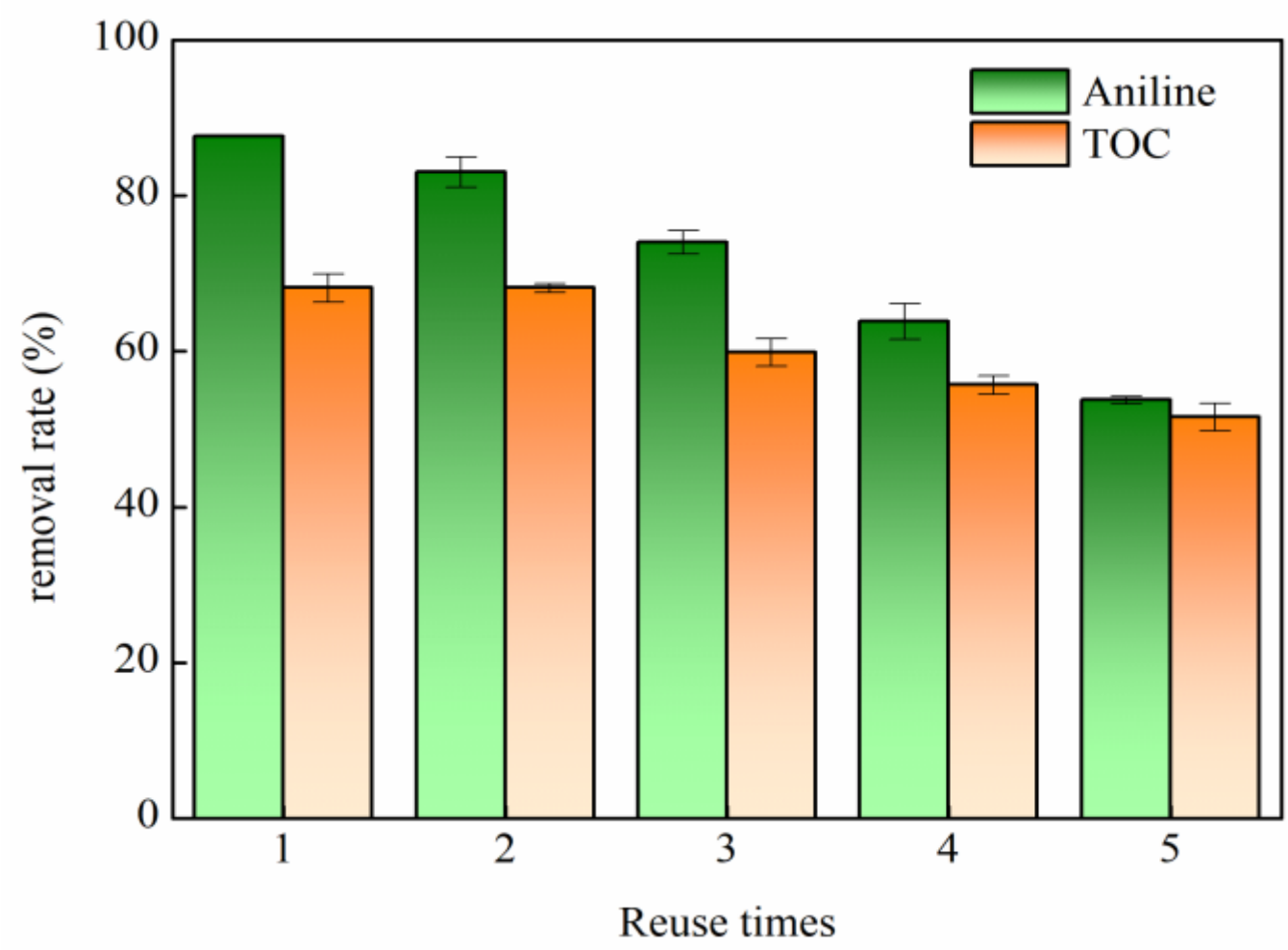

Figure 8

Reuse of CS in PS degradation AN ($[AN]_0$=100 mg·L^{-1}, $[PS]_0$=3 g·L^{-1}, $[CS]_0$=3 g·L^{-1} and reaction time = 2 h).